Journal of the Optical Society of America B
OPTICAL PHYSICS

Performance peculiarities of carbon-nanotube-based thin-film saturable absorbers for erbium fiber laser mode-locking

Alexander A. Krylov,[1,*] Stanislav G. Sazonkin,[2] Natalia R. Arutyunyan,[3,4] Vyacheslav V. Grebenyukov,[3] Anatoly S. Pozharov,[3] Dmitry A. Dvoretskiy,[2] Elena D. Obraztsova,[3,4] and Evgeny M. Dianov[1]

[1]Fiber Optics Research Center of the Russian Academy of Sciences, 38 Vavilov str., 119333 Moscow, Russia
[2]Bauman Moscow State Technical University, 2nd Bauman str. 5, 107005 Moscow, Russia
[3]A.M. Prokhorov General Physics Institute of the Russian Academy of Sciences, 38 Vavilov str., 119333 Moscow, Russia
[4]National Research Nuclear University MEPhI (Moscow Engineering Physics Institute), Kashirskoye shosse 31, 115409 Moscow, Russia
*Corresponding author: sokolak@mail.ru

Received 1 October 2015; revised 3 December 2015; accepted 3 December 2015; posted 8 December 2015 (Doc. ID 251118); published 7 January 2016

We have studied the saturation behavior of single-walled carbon-nanotube-based saturable absorbers (SWCNT-SAs) at different temperatures and SWCNT concentrations in the polymer matrix and tried to relate it to the mode-locked erbium-doped fiber laser performance. It has been observed that a modulation depth of SWCNT-SA transmission which we relate to the ground state recovery time monotonically decreases upon temperature growth. Comparing laser performance with different SWCNT-SAs, we suppose that the defects in the CNT lattice promote recovery acceleration resulting in shorter pulse generation as obtained for boron-nitride-doped SWCNTs. Moreover, for the first time, to the best of our knowledge, we have observed and studied the long-term relaxation of SWCNT-SA saturated transmission exhibiting temperature-dependent behavior.

OCIS codes: (140.4050) Mode-locked lasers; (320.7090) Ultrafast lasers; (160.4330) Nonlinear optical materials.

http://dx.doi.org/10.1364/JOSAB.33.000134

1. INTRODUCTION

At present, ultrashort pulse (USP) fiber laser sources attract much attention due to their prospective applications in science, medicine, and industry [1,2]. To date, USP generation has been efficiently realized using various mode-locking (ML) techniques [2,3]. Among them, nonlinear polarization evolution (NPE) [4] based on the fast nonlinear Kerr effect in fibers and various kinds of saturable absorbers (SAs) such as semiconductor saturable absorber mirror (SESAM) [5] and different carbon-based structures [single-walled carbon nanotubes (SWCNT), graphene, and others] [6,7] are the most favorable now for fiber laser mode-locking.

Compared to quantum-well-based SESAMs, SWCNT-SAs benefit from easier and cost-effective fabrication techniques, the possibility of being used in both linear and ring cavities, ultrafast carrier relaxation time [8], and significantly enhanced noise characteristics [9]. Furthermore, SWCNTs can be naturally dispersed in different polymer matrices forming high-optical-quality films that can be further built in the laser cavity without breaking the all-fiber setup as well as requiring mechanical or thermal adjustments [10,11,12]. Unlike SESAMs, CNT-based saturable absorbers exhibit saturable behavior over much wider spectral band (up to 500 nm and more) at the expense of the inherent distribution of SWCNTs' diameters and chiralities [6,10,11,13], which is quite favorable for wide-band photonic-switching applications [14,15].

Lower saturation power also with longer recovery time of SWCNT-SAs in comparison with NPE provides a significant reduction in the mode-locking threshold, thus facilitating a highly reliable start-up of USP generation. Moreover, being a naturally interferometric process, NPE is strongly susceptible to the environmental conditions (such as pressure and temperature) required for active stabilization system development (e.g., temperature control) for the stable long-term operation to be achieved. Thus, SWCNT-SAs, being free of this drawback, are highly promising for environmentally stable robust USP fiber laser development.

Up to now, various USP generation regimes have been realized through SWCNT-SA mode-locking of erbium-doped fiber lasers: conservative [16] and dissipative [17] solitons, stretched

[18] and chirped [16] pulses, and multi-gigahertz repetition frequency pulses [19]. Furthermore, SWCNT-SA can support higher-energy (up to 63 nJ) USP generation [20]. At the moment, as short as 66 fs pulses have been retrieved from the SWCNT-SA mode-locked erbium-doped all-fiber ring oscillator [21].

However, despite well-elaborated SWCNT-based film fabrication technologies, it is difficult to control such a crucial characteristic for laser mode-locking as an absorber response time during the SWCNT-SA fabrication process. As a matter of fact, the SWCNT-SA response time defined by complicated tube–tube interactions (excited-state energy is transferred to metallic NTs with further quenching) [8] strictly depends on the particular sample fabrication process [22]. Moreover, a polarization dependence of saturable absorption cannot be controlled as well since SWCNTs' orientations are randomly distributed. All of these features make SWCNT-SA characteristics as well as corresponding mode-locked laser performance absolutely unpredictable, thus impeding a realization of a reproducible USP generation.

Unfortunately, very few works provide research on the relationship between the SWCNT-SA parameters and the laser pulse characteristics observed [23,24,25,26,27], and there is nothing about SWCNT-SA behavior at different temperatures. Basically, linear characteristics such as small-signal absorption [23,24], SWCNT concentration [25,26], SWCNT film thickness [24,25,26], and nonsaturable losses [26,27] together with some nonlinear ones such as saturation power [27] and modulation depth of SA [26,27] are taken into consideration for describing an USP parameters' evolution. However, such a key feature for laser mode-locking as SWCNT-SA relaxation dynamics is now beyond the scope of these studies. Thus, it is of great importance to find an experimentally unambiguous relationship between saturation and relaxation characteristics of SWCNT-SA and a corresponding laser performance observed.

Here, we thoroughly explore saturation and relaxation behaviors of SWCNT-SAs at different temperatures and SWCNT concentrations in the polymer matrix and relate it to the generation characteristics of the SWCNT-SA mode-locked erbium-doped all-fiber soliton ring laser.

2. EXPERIMENTAL SETUP

A. SWCNT-SA Preparation

In this work we have studied four samples of SWCNT-based saturable absorbers. Three of them (samples #1–#3) contained pure SWCNTs with different concentrations, but the fourth one (marked as #BN) incorporated boron-nitride-doped SWCNTs (C:BNNTs).

The SWCNTs were synthesized by the arc discharge method in the helium atmosphere (with static pressure of 600 Torr) with the help of the Ni – Y_2O_3 catalyst (in weight proportion Ni:Y_2O_3:C – 1 : 1 : 2) [10]. Carbon nanotubes synthesized by this method have a more pronounced redshifted optical-absorption band comparing to the SWCNTs produced by the laser ablation, chemical vapor deposition, or high-pressure carbon monoxide techniques [28]. Stable suspensions of individual SWCNTs in a 1 wt.% aqueous solution of carboxymetylcellulose (CMC) have been prepared by ultrasonication followed by ultracentrifugation and a slow evaporation of the solvent [10]. Cellulose is an efficient surfactant and matrix material simultaneously. Due to this fact, the only two components (cellulose and SWCNTs) are necessary in the suspension to create high-optical-quality films further built in the laser cavity [10]. During the film fabrication procedure, different amounts of SWCNTs were taken to vary the SWCNT concentration in the resulting solution.

To produce C:BNNTs, the experimental setup was slightly modified. C:BNNTs were also synthesized using the arc discharge procedure in a vacuum chamber with a stationary He atmosphere at 420 Torr. At the same time, one of the electrodes had a cavity filled with a mixture of graphite (C), nickel (Ni), and yttrium oxide (Y_2O_3) powders at a ratio of 2:1:1 by mass, with an admixture of 5% boron nitride (BN, hexagonal phase) and 5% boron carbide (B_4C), by mass. This electrode was evaporated using a direct current arc at 105 A and 40 V [29].

The resulting soot was ultrasonicated using a Hielscher UP200H dispenser in deionized distilled H_2O with carboxymethilcellulose (CMC) acting as a surfactant. Ratios were 0.1% soot and 1% CMC, by mass. This suspension was ultracentrifuged at 150,000 g using a Beckman Coulter Maxima-E centrifuge, and the transparent part of suspension was extracted. Films were formed by drying this suspension of optical quality in a Petri dish at room temperature for 2 weeks as in the previous case.

BN incorporation into a CNT mesh is possible due to the same single-layer hexagonal lattice with almost the same spacing [30]. The effect of BN doping is in the bandgap energy (ΔE) increase for semiconducting NTs that accounts for a controllable blueshifting of the peak wavelength corresponding to the $S_1(E_{11})$ absorption band [29,30]. In addition, nonzero ΔE originates in metallic SWNTs. The increase of ΔE is supposed to arise from a contribution of two possible phenomena. One of them is SWNT synthesis with smaller diameters and the other is SWCNTs' electronic structure modification under BN incorporation [29,30]. Thus, through appropriate synthesis conditions, optical properties of C:BNNTs can be varied in a controllable way.

However, the content of B and N atoms in the resulting CNT mesh was too low (it was estimated to be less than 5%) to modify the CNT diameter and energy zone structure significantly. Thus, they can be considered as defects in the regular CNT lattice.

The thickness was about 50 μm for all films prepared, while SWCNT diameters estimated from the radial breathing mode (RBM) frequency positions in corresponding Raman spectra were distributed around 1.4 nm [31]. Small-signal transmission spectra of given samples are demonstrated in Fig. 1 [the resulting SWCNT concentration in the corresponding film (in wt.%) is given in parenthesis]. As it is seen, the spectral maxima of the $S_1(E_{11})$ absorption band is close to 1720 nm for the samples #1–#3. At the same time, the absorption maximum of the #BN sample turns out to be slightly blueshifted to the 1680 nm wavelength. A small-signal transmittance is varied from 54% (for the sample #BN) to 78% (for the sample #1) at the wavelength of 1560 nm that belongs to the Er-doped fiber amplification band. Moreover, Er-doped fiber laser wavelengths are significantly shorter than S_1 absorption peaks of the SWCNT-SAs employed, giving rise to the complicated two-stage ground-state recovery [8,22]. As expected, the transmission spectra of samples #1–#3 produced with the same SWCNTs have almost the same shape

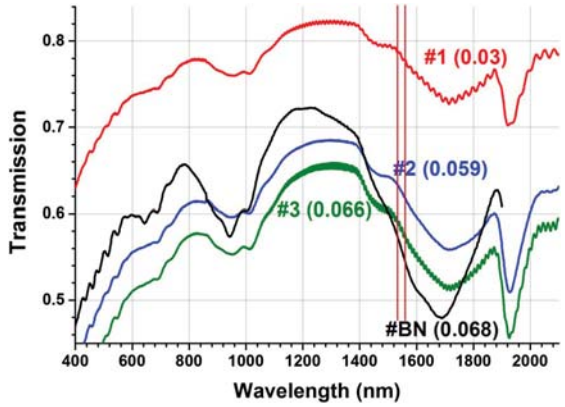

Fig. 1. Small-signal transmission spectra of CMC films with dispersed single-walled nanotubes (vertical lines correspond to 1532 and 1559 nm wavelengths).

which unambiguously indicates the concentration dependence of the small-signal absorption (larger SWCNT concentration corresponds to higher losses). Meanwhile, it would be quite interesting to compare Er-doped laser performance with samples #BN and #3 having close small-signal transmission values at the wavelength of 1560 nm.

B. Erbium-Doped Fiber Laser Setup for the Ground State Recovery Time Measurement

The mode-locked erbium-doped all-fiber ring laser scheme is shown in Fig. 2. The ring cavity was formed with a homemade 1.2 m long alumina-silicate erbium-doped fiber (EDF) with 10.6 μm mode field diameter and 5×10^{-3} refractive index difference (corresponding to the cutoff wavelength of $\lambda_c \approx 1340$ nm) having 11 dB/m small-signal absorption at 980 nm wavelength. EDF was pumped with a 980 nm, 200 mW single-mode laser diode (SM-LD) through the 980/1550 WDM. Group velocity dispersions (GVD) of EDF and passive SMF28 fibers were measured to be $\beta_2(\text{EDF}) = -21$ ps^2/km and $\beta_2(\text{SMF28}) = -24$ ps^2/km at 1560 nm wavelength, respectively.

A commercial fiber isolator (ISO) ensured unidirectional generation inside the cavity while the laser radiation was put out through a 3 dB fused fiber coupler. The polarization controller (PC) was also inserted into the ring to control a polarization state of the radiation.

CMC films (one or two units depending on the experiment) incorporating SWCNTs were fixed between two angular-polished ferrules of APC optical connectors to form the well-known robust saturable absorber incorporating carbon nanotubes (SAINT) module [6,16] further placed in the laser cavity in order to initiate mode-locked lasing.

Taking into account GVD values of different fibers composing a 3.3 m long ring, the total intracavity GVD value was calculated to be $D_T \approx -0.073$ ps^2. As a matter of fact, negative GVD supports a soliton-type USP generation as shown earlier [3,4]. Obviously, we keep in mind that being naturally stable pulses, solitons are resistant to perturbations caused by the cavity nonuniformity which might facilitate mode-locking realization for recovery time measurements [3,4].

The laser pulse width was retrieved from the pulse intensity autocorrelation measurements, while laser spectra were registered with the high-resolution ANDO spectrum analyzer. It should be mentioned that during laser experiments we tried to achieve a stable mode-locked lasing in a wide range of pump powers as possible for any SWCNT-SA used in order to get a full range of soliton pulse widths.

C. Experimental Setup for SWCNT-SA Saturation and Relaxation Measurements

The experimental scheme for SWCNT-SA saturation and relaxation measurements is shown in Fig 3. Probe radiation from the 120 fs 1.56 μm homemade Er-doped fiber laser passing through a tunable attenuator (TA) was split into two ports by means of the 20/80 fused fiber coupler. One port (20%) was a bias while the second port (80%) was spliced to the common SAINT module with one or two successively mounted CMC films under investigation. Taking into account dispersive broadening of the 120 fs pulse during its propagation along the fibers, the SAINT module was located immediately in the pulse "focus" point being 138 cm apart from the probe laser output. Signals from these ports were monitored with a highly sensitive power meter Coherent FieldMaxII.

We aimed to use as short probe pulses as possible to satisfy the condition of a slow saturable absorber [32] which implied a laser pulse width to be much shorter than the absorber recovery time. According to this assumption, optical losses l($l = 1 - T = 1 - E_p^{\text{out}}/E_p^{\text{in}}$) in SWCNT-SA depending on the input pulse energy E_p can be expressed as [32]

$$l = l_{\text{ns}} + \Delta T \cdot \frac{1 - \exp(-E_p/E_{\text{sat}})}{E_p/E_{\text{sat}}}. \quad (1)$$

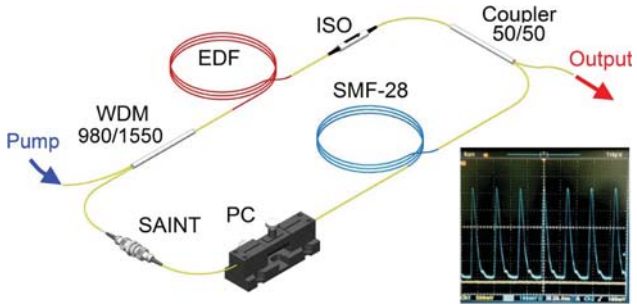

Fig. 2. Experimental setup of the mode-locked erbium-doped all-fiber soliton ring laser. Inset: highly stable pulse train.

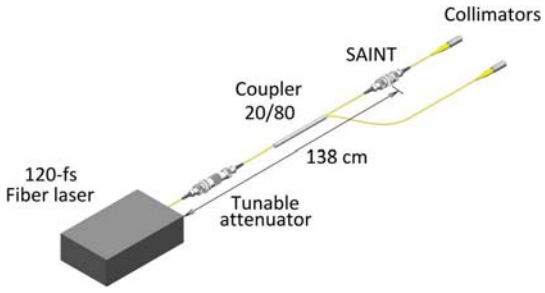

Fig. 3. Experimental setup for SWCNT-SA saturation and relaxation measurements.

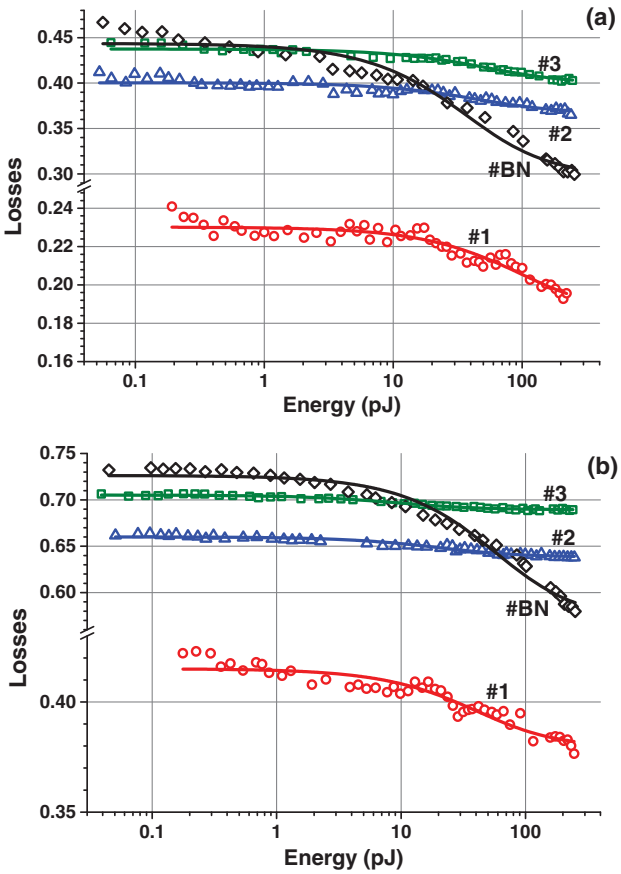

Fig. 4. Saturation behavior of SWCNT-SAs in (a) single-film and (b) double-film setups upon 120 fs USP excitation at 1560 nm.

Here, l_{ns} represents nonsaturable losses, ΔT is the modulation depth of the losses (transmission), and E_{sat} is the saturation energy that accounts for a saturation behavior in the case of a slow saturable absorber [32].

3. EXPERIMENTAL RESULTS

A. SWCNT-SA Saturation and Relaxation Measurements

Figure 4 shows the saturation behavior of all SWCNT-SA samples in the case of single- [Fig. 4(a)] and double- [Fig. 4(b)] CMC-film setups which are quite accurately approximated with Eq. (1). The resulting saturation characteristics are summarized in Table 1.

There are some noteworthy features arising from the measured SWCNT-SA saturation behavior. First of all, as it is observed for the samples #1–#3, SWCNT concentration increase does not lead to the corresponding growth of ΔT. Moreover, modulation depth for the double-film configuration is also reduced. Note that the highest reduction was obtained for the least transparent sample #3 (2.4×). On the contrary, ΔT for the sample #BN is almost the same for both single- and double-film setups. Figure 5 directly compares saturation behavior of single- and double-film SWCNT-SAs for the samples #BN and #3 [in this case, corresponding small-signal losses (l_0) were superposed]. In fact, not only modulation depth but also saturation energy significantly varies in the case of using sample #3. Thus, two CMC films installed together in the same SAINT module should be considered as one unique saturable absorber rather than two independent absorbers.

Further, we proceeded with a study of the SWCNT-SA saturation behavior at different temperatures. In these experiments, the SAINT module with the #BN sample inside was cooled down to 77 K (using liquid nitrogen) and heated up to 423 K (150°C). Figure 6 shows saturation curves measured at 77 K, 293 K (room temperature), and 423 K for boron-nitride-doped SWCNT-SA. First of all, CMC films with C:BNNTs dispersed demonstrate outstanding thermal stability and exhibit saturation behavior over a wide temperature range without film crushing. It is worth noting that an increase of small-signal losses (unsaturated losses) at 77 K is partially induced by the temperature-dependent losses of the FC/APC connection itself (SAINT module without CMC film) that was proved experimentally. Meanwhile, the saturation curve at 423 K almost fully originates from the temperature-dependent behavior of C:BNNTs in the CMC matrix that is justified by almost equal nonsaturable losses at room and high temperatures [$l_{ns}(423\ \mathrm{K}) = 28.9 \pm 0.3\%$, $l_{ns}(293\ \mathrm{K}) = 29.4 \pm 0.6\%$]. It is quite evident that ΔT remains almost unchanged ($\Delta T_{77} = 13.8 \pm 0.5\%$) at 77 K and is noticeably reduced ($\Delta T_{423} = 9.8 \pm 0.3\%$) at 423 K. However, E_{sat} is not varied sufficiently, ranging from 19 ± 2 pJ at 77 K to 26 ± 3 pJ at 423 K. Moreover, it was observed that saturation behavior is not recovered after C:BNNTs-SA cooling from 423 K to room temperature. On the contrary, the saturation curve in this case almost fully coincides with one measured at 423 K. Thus, we suppose irreversible modification of the SWCNT-SA structure

Table 1. SWCNT-SA Characteristics Together with the Corresponding Laser Parameters

Sample[a]	#1(1)	#1(2)	#2(1)	#2(2)	#3(1)	#3(2)	#BN(1)	#BN(2)
l_{ns}, %	18.4 ± 0.5	37.9 ± 0.2	36.6 ± 0.3	63.8 ± 0.1	39.9 ± 0.2	68.92 ± 0.03	29.4 ± 0.6	56.9 ± 0.6
ΔT, %	4.6 ± 0.5	3.6 ± 0.2	3.4 ± 0.2	2.20 ± 0.08	3.9 ± 0.2	1.60 ± 0.03	14.9 ± 0.6	15.8 ± 0.6
E_{sat}, pJ	55 ± 13	23 ± 4	26 ± 6	11.6 ± 1.5	30 ± 4	5.4 ± 0.5	21 ± 3	33 ± 4
T_0, %	77	58.5	60	34	56.2	29.5	55.6	27.4
F_{sat}, μJ/cm^2	62	26	29	13	34	6.1	24	37
E_p^{max}, pJ	34.8	91.7	64.6	19.1	74.7	23.7	81.5	72.3
P_{av}^{max}, mW	2	5.3	3.7	1.1	4.3	1.4	5	4.4
τ_p^{min}, ps	1.06	0.68	0.76	1.71	0.72	1.57	0.5	0.46
P_{pump}, mW	53	94	77.4	66.6	85.6	74.1	85	100

[a]Number in parenthesis denotes the number of films installed.

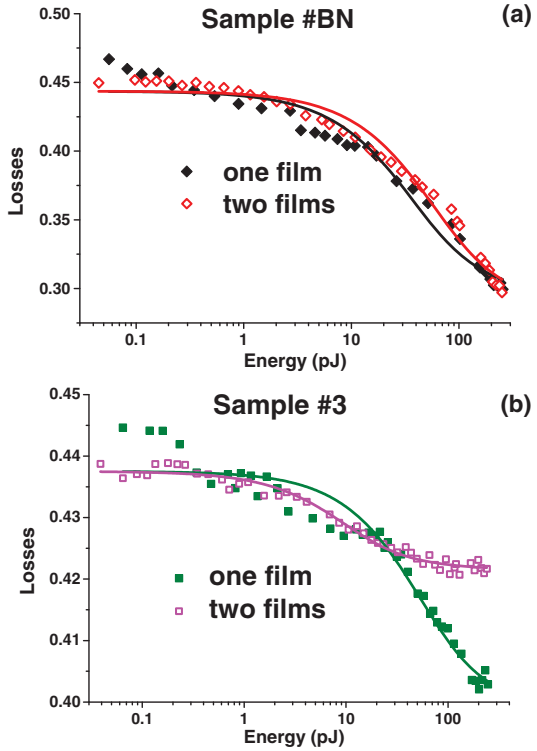

Fig. 5. Comparison of the saturation behavior of single- and double-film SWCNT-SAs for the samples (a) #BN and (b) #3.

upon its irradiation at 423 K followed by the modification of the SWCNT-SA saturation behavior.

It should be noted that previous experiments were conducted using fresh (untested) CMC films. Meanwhile, it is interesting to repeat saturation measurements immediately after the full saturation has been reached. The lowermost curve (olive) in Fig. 6 demonstrates the result of this experiment at room temperature. Evidently, C:BNNTs-SA transmission does not relax to its initial level that is inherent to the fresh film. At the same time, the initial saturation behavior was almost fully recovered within 24 h. This phenomenon was observed for all samples used. Therefore, we suppose the existence of long-term relaxation of SWCNT-SA transmission that significantly modifies its saturation behavior. To explore long-term relaxation, we measured the evolution of a small-signal transmission of SWCNT-SA with time immediately after fresh SWCNT-SA had been fully saturated. The experimental setup was the same as that used in saturation measurements (Fig. 3), but the energy of a probe pulse was fixed at 0.1 pJ to eliminate additional saturation of the SWCNT-SA.

Figure 7 presents the long-term relaxation for the sample #BN at different temperatures. Experimental data were fitted with decaying exponential functions with time constants equal to 37 ± 6 min (44 ± 2 min for sample #1) and 6.2 ± 1.3 min for 293 and 423 K, respectively. Being too slow, relaxation behavior at 77 K was approximated with a line having very small slope. Actually, the initial (unsaturated) SWCNT-SA transmission is almost fully recovered in the case of 293 and 423 K but this is not the case for 77 K. Here, the transmission value persisted even after following annealing at 150°C as if SWCNT-SA remains almost fully saturated. Thus, SWCNT-SA irradiation at 77 K also leads to irreversible changes of its structure. It should be mentioned here that the same behavior was observed for PVA-based films with SWCNTs dispersed during saturation measurements in the 2 μm spectral band [33]. However, long-term relaxation was not studied there.

Since nonsaturable losses remain almost unchanged [$l_{ns}(\mathrm{sat}) = 29.2 \pm 0.5\%$], it is quite reasonable to relate the long-term relaxation of SWCNT-SA transmission to some processes that occurred in carbon nanotube bundles rather than the polymer matrix itself. It was shown experimentally by Ahir *et al.* [34] that IR light irradiation of SWCNT-based films causes fully reversible additional stress (photomechanical actuation) exhibiting long-term relaxation with the same exponential behavior (at room temperature) that can be possibly described with a CNT networks contraction. Thus, we suggest that the long-term relaxation of SWCNT-SA transmission can also be associated with the effect of CNT networks contraction upon USP irradiation, at least at room temperature [34]. Of course, the relation between a long-term relaxation of SWCNT-SA transmission and a CNT networks contraction should be further proved experimentally.

In general, there exist two channels of saturated transmission relaxation. One of them is well-known ultrafast relaxation responsible for the laser mode-locking initiation (with a response

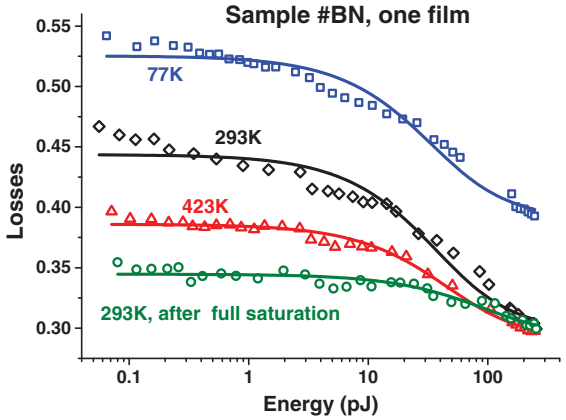

Fig. 6. Saturation behavior of the #BN sample at different temperatures.

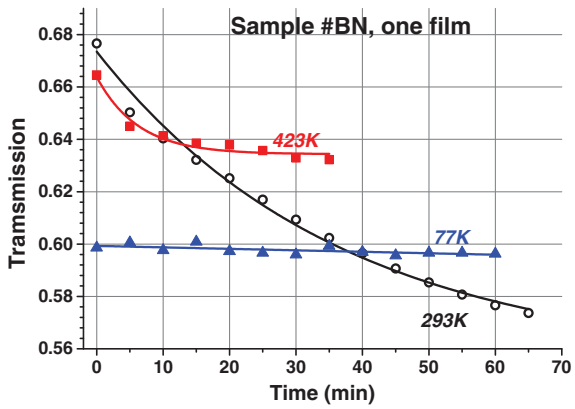

Fig. 7. Long-term relaxation of the small-signal transmission for the sample #BN at different temperatures.

time of ~1 ps), but the other channel is long-term relaxation (with ~10 min response) having evident temperature-dependent behavior that was observed and studied in this work. It is quite evident that the starting point of the blue curve in Fig. 7 (77 K) almost coincides with the finishing point of the corresponding saturation curve in Fig. 6 which means negligible modulation depth responsible for the ultrafast response at the cryogenic temperature. However, at both room and high temperatures a fast relaxation channel undoubtedly exists.

Obviously, due to the long-term relaxation the effective modulation depth ΔT^{eff} corresponded to the fast response is significantly reduced (as it follows from Fig. 6, $\Delta T^{\text{eff}} = 5.3 \pm 0.5\%$ in the case of the #BN sample at 293 K) with simultaneous saturation energy growth ($E_{\text{sat}}^{\text{eff}} = 52 \pm 14$ pJ) which can undoubtedly affect SWCNT-SA performance as a laser mode-locker.

B. Ground State Recovery Time Measurements for SWCNTs

Stable single-pulse, self-starting CW ML generation was realized in the laser depicted in Fig. 2 with all SWCNT-SA samples previously described (in both single- and double-CMC film configurations) at pump powers in the range of 53 to 100 mW. The pulse repetition frequency was close to 60.8 MHz being in agreement with a cavity length of 3.3 m. As expected, an influence of PC adjustments on the laser performance was negligible proving polarization independence of SWCNT-SAs used. Moreover, SWCNT-SAs were not damaged even at the highest pulse energies which implied pulse energy limitation arising from SWCNT-SA performance peculiarities only. The highest output laser characteristics (pulse energy $E_p^{\max}$, average power $P_{\text{av}}^{\max}$ also with the shortest pulse width $\tau_p^{\min}$) measured for each SWCNT-SA are presented in Table 1 for comparison.

Figure 8 demonstrates laser pulse-width dependence on the corresponding pulse energy $\tau_p(E_p)$. Taking into account soliton pulse behavior (according to the soliton area theorem) it is reasonable to expect pulse-width reduction with a pulse energy growth, as shown in Fig. 8. However, it turns out that experimental data obtained for the samples #1–#3 (in both single- and double-film setups) can be carefully approximated with one decaying exponential function $\tau_p = \tau_0 + A \cdot \exp(-E_p/E_0)$

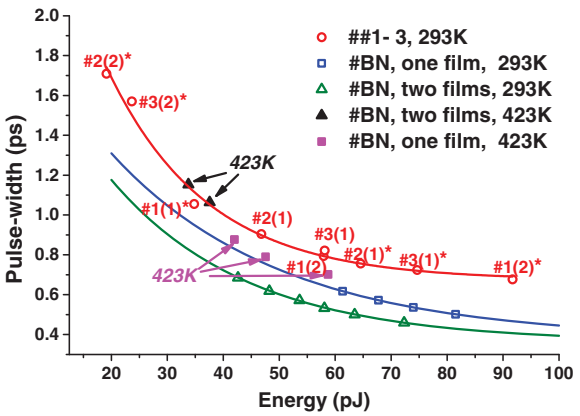

Fig. 8. Laser pulse-width evolution upon pulse energy growth (asterisk designates a point with highest energy archived for a given SA).

with an asymptote $\tau_0 = 673 \pm 36$ fs. Moreover, it is quite interesting that despite very low modulation depths measured for the samples #2 and #3 in the double-film configuration ($\Delta T_{2(2)}^{\text{eff}} < 2.2\%$, $\Delta T_{3(2)}^{\text{eff}} < 1.6\%$), stable ML generation was realized, though with small pulse energies of ≈20 pJ. This result can be ascribed to the significant reduction of the saturation energy (and saturation power accordingly) for these samples ($E_{\text{sat}}^{2(2)} = 11.6$ pJ, $E_{\text{sat}}^{3(2)} = 5.4$ pJ) which implies a strong saturation of SWCNT-SA at a very low pulse energy [that is clearly seen in Fig. 5(b) comparing saturation curves for single- and double-film setups] followed by ML collapsing into multipulse generation [32,35]. However, the shortest pulse width ($\tau_{\min} = 677$ fs) together with the highest pulse energy ($E_{\max} = 92$ pJ) were obtained using sample #1 in the double-film configuration with ΔT and E_s being lower if compared to the corresponding single-film setup (see Table 1).

In the case of the sample #BN at room temperature, $\tau_p(E_p)$ dependences were separately fitted with decaying exponential functions for single- and double-film setups giving τ_0 values equal to $\tau_0^{(1)} = 379 \pm 1$ fs and $\tau_0^{(2)} = 363 \pm 13$ fs, respectively. Unfortunately, strong SWCNT-SA saturation ($s = E_p/E_{\text{sat}} \approx 3$) prevents further pulse energy growth and, as a result, corresponding pulse-width shortening. Unlike the laser with samples #1–#3, single-pulse ML generation collapses in this case into the Q switch one rather than multipulsation which we ascribe to the long-term relaxation influence. Indeed, the SA modulation depth responsible for ultrafast relaxation is significantly reduced resulting in the severe Q switching instability growth followed by ML crushing.

On the basis of previous analysis, it is possible to associate τ_0 with SWCNT-SA ground state recovery time τ_r, $\tau_0 \sim \tau_r$. It is quite a reasonable assumption taking into account that samples #1–#3 were fabricated during one technological process which implied the same (or close) τ_r for them. As a matter of fact, SWCNT-SA relaxation consists of two processes determined by fast recovery time τ_f (corresponding to the intraband carrier transitions) and slow recovery τ_s (attributed to the interband transitions–carriers recombination) [8,22]. As shown in [22], $\tau_f \sim 200$ fs while τ_s was close to 1 ps for arc discharge SWCNTs in the CMC polymer matrix. Thus, it is possible to consider τ_s which we relate to the obtained τ_0 value being mainly responsible for the laser pulse-width limitation. It should be stressed that defects in the CNT mesh (B and N atoms) promote SA response acceleration resulting in shorter pulse generation as observed for the #BN sample. Meanwhile, it is like an ion bombing of as-grown SESAMs aiming at the response time shortening through a defects creation [5]. Moreover, larger ΔT could also be associated with smaller τ_s, thus providing a good criterion for an appropriate SWCNT-SA choice.

It is worth noting here that the shortest pulse width $\tau_{\min}$ retrieved from a soliton fiber laser is limited by the total cavity dispersion D_T according to the following expression [36]:

$$\tau_{\min} \cong 0.752\sqrt{|D_T|}. \quad \textbf{(2)}$$

Taking into account the cavity dispersion value $D_T \approx -0.073$ ps^2, the shortest pulse width inherent to the given cavity amounts to $\tau_{\min} \approx 200$ fs which is significantly shorter than both τ_p and τ_0 for all SWCNT-SA used. Thus,

the ground state recovery time τ_s together with a strong saturation of SWCNT-SA primarily limit soliton pulse-width shortening and corresponding pulse energy growth as well.

It is worth noting that a laser pulse width could be controlled via pulse energy variation in the range from 1.7 ps to 459 fs (2.8× ratio) using different CNT-SAs. However, a more flexible way of pulse-width tuning comes from a tunable fiber Bragg grating implementation in the CNT-SA mode-locked Er-doped fiber laser which gives more than a 20× pulse-width ratio [15].

For further examination of the pulse behavior, we studied the evolution of the inverse spectrum FWHM ($\Delta\lambda^{-1}$) together with time-bandwidth product (TBP $= \Delta\nu \cdot \tau_p$) with respect to the pulse energy, as shown in Fig. 9. It is interesting that the generation wavelength λ_0 is switched from 1559 to 1532 nm depending on the l_0 value (if $l_0 < 3$ dB then $\lambda_0 \approx 1559$ nm, otherwise $\lambda_0 \approx 1532$ nm). As observed for $\tau_p(E_p)$ dependence, $\Delta\lambda^{-1}(E_p)$ is also characterized by decaying exponential behavior for all SWCNT-SA samples used. It is not surprising taking into consideration a TBP value that is close to 0.4 and slightly increases during pulse energy growth. Thus, it is evident from Figs. 8 and 9 that laser pulse parameters are primarily determined by SWCNT-SA saturation and relaxation behaviors. Nonetheless, in spite of both $\tau_p(E_p)$ dependence and *TBP* values that differ from those inherent to fundamental solitons ($\tau_p \propto 1/E_p$, TBP $= 0.315$), soliton effects play a significant role during pulse propagation along the cavity. First, it is confirmed by means of a careful approximation of generated spectra of both shortest and longest pulses with a corresponding soliton function [$P(\omega) \propto \mathrm{sech}^2(\omega)$] [3–6,16,33,36], as shown in Fig. 10. In addition, a smooth pedestal-free soliton-type autocorrelation trace (see the inset in Fig. 10) also proves the noticeable role of the soliton effect during pulse propagation along a cavity.

Moreover, as shown in the inset of Fig. 10, a very weak side peak also with a narrow peak at ≈1555 nm are observed in the shortest pulse spectrum. This side peak could be naturally associated with the well-known Kelly side-band inherent to the spectra of soliton fiber lasers [3–5,33,36]. Obviously, it is strongly weakened due to the filtering effect in the CNT-SA [37]. Indeed, weak CW radiation of dispersive waves shed

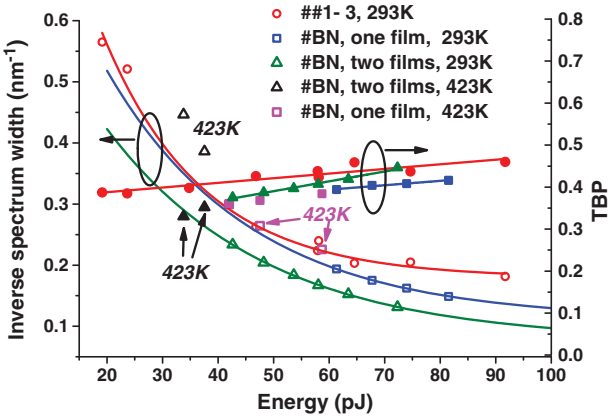

Fig. 9. Inversed spectrum FWHM together with time-bandwidth product versus pulse energy.

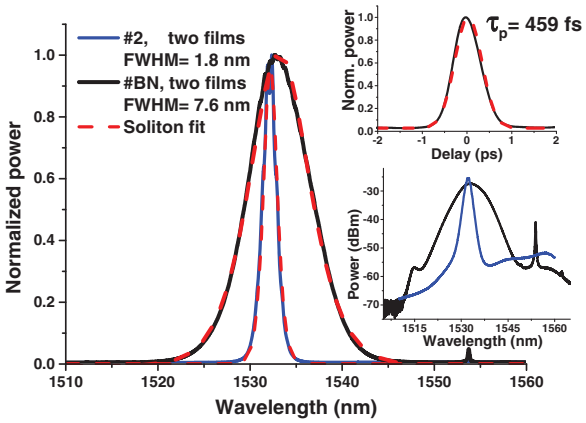

Fig. 10. Spectra of the shortest (black curve) and longest (blue curve) pulses together with soliton-type approximation (dashed curves). Insets: autocorrelation trace of the shortest pulse together with its soliton-type fit (dashed curve) in the top plot and pulse spectra in the logarithmic scale in the bottom plot.

by the soliton propagating along the cavity could be absorbed in the CNT-SA without its saturation. The well-resolved peak at ≈1555 nm could be attributed to the *Q* switching instability of USP generation with the highest energy and shortest pulse width that was discussed above.

Further, we studied the laser performance upon SWCNT-SA temperature variation. In these experiments, the intracavity SAINT module with the sample #BN inside (one or two films were installed) was cooled down to 77 K and heated up to 423 K.

First of all, mode-locked operation was achieved at 77 K but degraded into *Q* switch irreversibly. Possibly the fast relaxation channel responsible for a laser mode-locking collapses due to some structural changes of SWCNT film at low temperature (SWCNT-SA stays almost fully saturated as observed previously, see Fig. 7). However, pulse characteristics were close to those attained at room temperature at the same pump power (69 mW). It means that the ground state recovery time keeps its value unchanged.

At high temperature (423 K) stable single-pulse mode-locking was realized for both single- and double-film setups at pump powers ranging from 50 to 73 mW. However, as seen in Fig. 8, pulse characteristics (pulse width also with pulse energy) significantly worsened especially in the case of two films. Undoubtedly, such a behavior originates from modified saturation and relaxation properties of SWCNTs at high temperature (see Fig. 6). Since modulation depth (ΔT) was shown to drop with temperature growth and taking into account the relation between ΔT and response time τ_s, pulse characteristics worsening could be assigned to the τ_s increase upon SA heating.

As a matter of fact, intraband relaxation dynamics was experimentally and theoretically proved to be both acoustic and optical phonon assisted [38,39]. However, the nature of an interband relaxation (carriers' recombination) is still argued about [40]. It was stated previously that the primary recombination channel in bundled SWCNT samples through tube–tube interactions (charge transfer mechanism) between semiconducting and metallic NTs was independent of temperature [8].

However, our measurements evidence in favor of temperature-dependent ground state recovery which implies CNT phonon involvement. Of course, more profound research targeting the ground state recovery investigation should be further provided to clear up this ambiguity.

As it follows from Fig. 8, laser pulse energy is limited by ≈100pJ due to the strong saturation of SWCNT-SA. At the same time, SWCNT-SA provides reliable ML start-up with low pulse energies owing to the rather low saturation energy and picosecond-level response time. This feature can be successfully used in hybridly mode-locked lasers based on the co-action of slow (SWCNT-SA) and fast (nonlinear polarization evolution [33,41] or nonlinear amplifying loop mirror [6]) saturation mechanisms. In this case SWCNT-SA not only facilitates mode-locking start-up but also provides a nonlinear filtering and spurious CW radiation suppression [37,41], significantly improving laser performance. High-quality USP shaping, in turn, primarily occurs due to the fast saturation mechanism.

4. CONCLUSIONS

In conclusion, we have thoroughly investigated SWCNT-SA saturation behavior at different temperatures and SWCNT concentrations in the polymer matrix with relation to mode-locking performance of the Er-doped fiber soliton laser. The following results were obtained:

1. It was shown that SWCNT concentration increase does not lead to the corresponding growth of the modulation depth of the SA transmission. Moreover, the modulation depth is kept at the same level or even reduced for the double-film setup. Thus, two films installed together in the same SAINT module should be considered as one unique saturable absorber.
2. During SWCNT-SA saturation measurements we observed the long-term relaxation of SWCNT-SA saturated transmission exhibiting strongly temperature-dependent behavior that could be associated with CNT networks contraction. Moreover, due to the long-term relaxation the effective modulation depth corresponding to the fast response is significantly reduced which undoubtedly affect SWCNT-SA performance as a laser mode-locker.
3. It was shown that soliton pulse-width dependence on soliton energy could be fitted with a decaying exponential function with an asymptote τ_0 related to the SWCNT-SA ground state recovery time τ_s. Thus, we suggest that the ground state recovery time together with a strong SWCNT-SA saturation primarily limit soliton pulse width and energy.
4. Comparing laser performance with different SWCNT-SAs we observed that incorporating boron-nitride-in SWCNTs promote SA response acceleration resulting in shorter pulse generation.
5. We observed the temperature-dependent character of the ground state recovery process according to the temperature dependence of SWCNT-SA mode-locking performance. However, further detailed investigations should be carried out.

We believe that such advantages of SWCNT-SAs as low mode-locking thresholds also with a reliable ML start-up would be quite beneficial for using them in hybrid mode-locking laser setups giving a significant improvement in laser performance.

Funding. Russian Scientific Foundation (14-22-00-243).

Acknowledgment. The authors are grateful to M. M. Bubnov and M. E. Likhachev from FORC RAS for active fiber provision. The authors also thank A. K. Senatorov for fiber GVD measurements and M. A. Chernysheva from FORC RAS also with B. L. Davydov from IRE RAS for technical support.

REFERENCES

1. W. Sibbett, A. A. Lagatsky, and C. T. A. Brown, "The development and application of femtosecond laser systems," Opt. Express **20**, 6989–7001 (2012).
2. M. E. Fermann, A. Galvanauskas, and G. Sucha, *Ultrafast Lasers: Technology and Applications* (Marcel Dekker, 2001).
3. M. E. Fermann, "Ultrafast fiber laser technology," IEEE J. Sel. Top. Quantum Electron. **15**, 191–206 (2009).
4. L. E. Nelson, D. J. Jones, K. Tamura, H. A. Haus, and E. P. Ippen, "Ultrashort-pulse fiber ring lasers," Appl. Phys. B **65**, 277–294 (1997).
5. O. Okhotnikov, A. Grudinin, and M. Pessa, "Ultra-fast fibre laser systems based on SESAM technology: new horizons and applications," New J. Phys. **6**, 177 (2004).
6. S. Yamashita, A. Martinez, and B. Xu, "Short pulse fiber lasers mode-locked by carbon nanotubes and graphene," Opt. Fiber Technol. **20**, 702–713 (2014).
7. H. G. Rosa, D. Steinberg, J. D. Zapata, L. A. M. Saito, A. M. Cárdenas, J. C. V. Gomes, and E. A. Thoroh De Souza, "Raman mapping characterization of all-fiber CVD monolayer graphene saturable absorbers for erbium-doped fiber laser mode locking," J. Lightwave Technol. **33**, 4118–4123 (2015).
8. J.-S. Lauret, C. Voisin, G. Cassabois, C. Delalande, P. Roussignol, O. Jost, and L. Capes, "Ultrafast carrier dynamics in single-wall carbon nanotubes," Phys. Rev. Lett. **90**, 057404 (2003).
9. K. Wu, X. Li, Y. Wang, Q. J. Wang, P. Ping Shum, and J. Chen, "Towards low timing phase noise operation in fiber lasers mode locked by graphene oxide and carbon nanotubes at 1.5 μm," Opt. Express **23**, 501–511 (2015).
10. A. I. Chernov, E. D. Obraztsova, and A. S. Lobach, "Optical properties of polymer films with embedded single-wall nanotubes," Phys. Status Solidi B **244**, 4231–4235 (2007).
11. M. A. Solodyankin, E. D. Obraztsova, A. S. Lobach, A. I. Chernov, A. V. Tausenev, V. I. Konov, and E. M. Dianov, "1.93 mm mode-locked thulium fiber laser with a carbon nanotube absorber," Opt. Lett. **33**, 1336–1338 (2008).
12. R. M. Gerosa, D. Steinberg, H. G. Rosa, C. Barros, C. J. S. de Matos, and E. A. T. de Souza, "CNT film fabrication for mode-locked Er-doped fiber lasers: the droplet method," IEEE Photon. Technol. Lett. **25**, 1007–1010 (2013).
13. T. Hasan, Z. Sun, P. Tan, D. Popa, E. Flahaut, E. J. R. Kelleher, F. Bonaccorso, F. Wang, Z. Jiang, F. Torrisi, G. Privitera, V. Nicolosi, and A. C. Ferrari, "Double-wall carbon nanotubes for wide-band, ultrafast pulse generation," ACS Nano **8**, 4836–4847 (2014).
14. X. Liu, D. Han, Z. Sun, C. Zeng, H. Lu, D. Mao, Y. Cui, and F. Wang, "Versatile multi-wavelength ultrafast fiber laser mode-locked by carbon nanotubes," Sci. Rep. **3**, 2718 (2013).
15. X. Liu and Y. Cui, "Flexible pulse-controlled fiber laser," Sci. Rep. **5**, 9399 (2015).
16. M. A. Chernysheva, A. A. Krylov, A. A. Ogleznev, N. R. Arutyunyan, A. S. Pozharov, E. D. Obraztsova, and E. M. Dianov, "Control over the performance characteristics of a passively mode-locked erbium-doped fibre ring laser," Quantum Electron. **43**, 691–698 (2013).
17. N. Nishizawa, Y. Nozaki, E. Itoga, H. Kataura, and Y. Sakakibara, "Dispersion-managed, high-power, Er-doped ultrashort-pulse fiber laser using carbon-nanotube polyimide film," Opt. Express **19**, 21874 (2011).
18. W. S. Kwon, H. Lee, J. H. Kim, J. Choi, K.-S. Kim, and S. Kim, "Ultrashort stretched-pulse L-band laser using carbon-nanotube saturable absorber," Opt. Express **23**, 7779–7785 (2015).

19. A. Martinez and S. Yamashita, "Multi-gigahertz repetition rate passively modelocked fiber lasers using carbon nanotubes," Opt. Express **19**, 6155–6163 (2011).
20. D. Popa, Z. Sun, F. Torrisi, T. Hasan, F. Wang, and A. C. Ferrari, "Generation of 63-nJ pulses from a fiber oscillator mode-locked by nanotubes," in *Conference on Lasers and Electro-Optics (CLEO)* (Optical Society of America, 2010), paper JTuD50.
21. Z. Yu, Y. Wang, X. Zhang, X. Dong, J. Tian, and Y. Song, "A 66 fs highly stable single wall carbon nanotube mode locked fiber laser," Laser Phys. **24**, 015105 (2014).
22. E. A. Obraztsova, L. Luer, E. D. Obraztsova, A. Chernov, D. Brida, D. Polli, and G. Lanzani, "Effect of environment on ultrafast photoexcitation kinetics in single-wall carbon nanotubes," Phys. Status Solidi B **247**, 2831–2834 (2010).
23. F. Shohda, M. Nakazawa, J. Mata, and J. Tsukamoto, "A 113 fs fiber laser operating at 1.56 μm using a cascadable film-type saturable absorber with P3HT-incorporated single-wall carbon nanotubes coated on polyamide," Opt. Express **18**, 9712–9721 (2010).
24. H. G. Rosa and E. A. De Souza, "Bandwidth optimization of a carbon nanotubes mode-locked erbium-doped fiber laser," Opt. Fiber Technol. **18**, 59–62 (2012).
25. J.-C. Chiu, Y.-F. Lan, C.-M. Chang, X.-Z. Chen, C.-Y. Yeh, C.-K. Lee, G.-R. Lin, J.-J. Lin, and W.-H. Cheng, "Concentration effect of carbon nanotube based saturable absorber on stabilizing and shortening mode-locked pulse," Opt. Express **18**, 3592–3600 (2010).
26. J.-C. Chiu, C.-M. Chang, B.-Z. Hsieh, S.-C. Lin, C.-Y. Yeh, G.-R. Lin, C.-K. Lee, J.-J. Lin, and W.-H. Cheng, "Pulse shortening mode-locked fiber laser by thickness and concentration product of carbon nanotube based saturable absorber," Opt. Express **19**, 4036–4041 (2011).
27. Á. Szabó and Z. Várallyay, "Numerical study on the saturable absorber parameter selection in an erbium fiber ring oscillator," IEEE Photon. Technol. Lett. **24**, 122–124 (2012).
28. C. Journet, W. K. Maser, P. Bernier, A. Loiseau, M. Lamy de la Chapelle, S. Lefrant, P. Deniard, R. Lee, and J. E. Fischer, "Large-scale production of single-walled carbon nanotubes by the electric-arc technique," Nature **388**, 756–758 (1997).
29. V. V. Grebenyukov, E. D. Obrazsova, N. R. Arutyunyan, S. N. Bokova, and A. S. Pozharov, "Optical studies of single-walled nanotubes synthesized from C:BN:B_4C catalytic mixtures," J. Nanoelectron. Optoelectron. **4**, 281–285 (2009).
30. N. R. Arutyunyan, R. Arenal, E. D. Obraztsova, O. Stephan, A. Loiseau, A. S. Pozharov, and V. V. Grebenyukov, "Incorporation of boron and nitrogen in carbon nanomaterials and its influence on their structure and opto-electronical properties," Carbon **50**, 791–799 (2012).
31. S. N. Bokova, V. I. Konov, E. D. Obraztsova, A. V. Osadchy, A. S. Pozharov, and S. V. Terekhov, "Laser-induced effects in Raman spectra of single-wall carbon nanotubes," Quantum Electron. **33**, 645–650 (2003).
32. R. Paschotta and U. Keller, "Passive mode locking with slow saturable absorbers," Appl. Phys. B **73**, 653–662 (2001).
33. M. A. Chernysheva, A. A. Krylov, C. Mou, R. N. Arif, A. G. Rozhin, M. H. Rmmeli, S. K. Turitsyn, and E. M. Dianov, "Higher-order soliton generation in hybrid mode-locked thulium-doped fiber ring laser," IEEE J. Sel. Top. Quantum Electron. **20**, 1100908 (2014).
34. S. V. Ahir, E. M. Terentjev, S. X. Lu, and B. Panchapakesan, "Thermal fluctuations, stress relaxation, and actuation in carbon nanotube networks," Phys. Rev. B **76**, 165437 (2007).
35. U. Keller, K. J. Weingarten, F. X. Kärtner, D. Kopf, B. Braun, I. D. Jung, R. Fluck, C. Hönninger, N. Matuschek, and J. Aus der Au, "Semiconductor saturable absorber mirrors (SESAM's) for femtosecond to nanosecond pulse generation in solid-state lasers," IEEE J. Sel. Top. Quantum Electron. **2**, 435–453 (1996).
36. V. J. Matsas, W. H. Loh, and D. J. Richardson, "Self-starting, passively mode-locked Fabry–Perot fiber soliton laser using nonlinear polarization evolution," IEEE Photon. Technol. Lett. **5**, 492–494 (1993).
37. S. Kim, Y. Kim, J. Park, S. Han, S. Park, Y.-J. Kim, and S.-W. Kim, "Hybrid mode-locked Er-doped fiber femtosecond oscillator with 156 mW output power," Opt. Express **20**, 15054–15060 (2012).
38. T. Hertel, R. Fasel, and G. Moos, "Charge-carrier dynamics in single-wall carbon nanotube bundles: a time-domain study," Appl. Phys. A **75**, 449–465 (2002).
39. C. Köhler, T. Watermann, and E. Malic, "Time- and momentum-resolved phonon-induced relaxation dynamics in carbon nanotubes," J. Phys. **25**, 105301 (2013).
40. A. Gambetta, G. Galzerano, A. G. Rozhin, A. C. Ferrari, R. Ramponi, P. Laporta, and M. Marangoni, "Sub-100 fs two-color pump-probe spectroscopy of single wall carbon nanotubes with a 100 MHz Er-fiber laser system," Opt. Express **16**, 11727–11734 (2008).
41. D. S. Chernykh, A. A. Krylov, A. E. Levchenko, V. V. Grebenyukov, N. R. Arutunyan, A. S. Pozharov, E. D. Obraztsova, and E. M. Dianov, "Hybrid mode-locked erbium-doped all-fiber soliton laser with a distributed polarizer," Appl. Opt. **53**, 6654–6662 (2014).